Altered Visual Function in a Larval Zebrafish Knockout of Neurodevelopmental Risk Gene *pdzk1*

Jiaheng Xie,[1] Patricia R. Jusuf,[1] Bang V. Bui,[2] Stefanie Dudczig,[1] Tamar E. Sztal,[3] and Patrick T. Goodbourn[4]

[1]School of BioSciences, The University of Melbourne, Melbourne, Australia
[2]Department of Optometry and Vision Sciences, The University of Melbourne, Melbourne, Australia
[3]School of Biological Sciences, Monash University, Melbourne, Australia
[4]Melbourne School of Psychological Sciences, The University of Melbourne, Melbourne, Australia

Correspondence: Patrick T. Goodbourn, Melbourne School of Psychological Sciences, The University of Melbourne, VIC 3010, Australia;
p.goodbourn@unimelb.edu.au.

Received: October 19, 2020
Accepted: February 24, 2021
Published: March 22, 2021

Citation: Xie J, Jusuf PR, Bui BV, Dudczig S, Sztal TE, Goodbourn PT. Altered visual function in a larval zebrafish knockout of neurodevelopmental risk gene *pdzk1*. *Invest Ophthalmol Vis Sci*. 2021;62(3):29.
https://doi.org/10.1167/iovs.62.3.29

Purpose. The human *PDZK1* gene is located in a genomic susceptibility region for neurodevelopmental disorders. A genome-wide association study identified links between *PDZK1* polymorphisms and altered visual contrast sensitivity, an endophenotype for schizophrenia and autism spectrum disorder. The PDZK1 protein is implicated in neurological functioning, interacting with synaptic molecules including postsynaptic density 95 (PSD-95), *N*-methyl-D-aspartate receptors (NMDARs), corticotropin-releasing factor receptor 1 (CRFR1), and serotonin 2A receptors. The purpose of the present study was to elucidate the role of PDZK1.

Methods. We generated *pdzk1*-knockout (*pdzk1*-KO) zebrafish using CRISPR/Cas-9 genome editing. Visual function of 7-day-old fish was assessed at behavioral and functional levels using the optomotor response and scotopic electroretinogram (ERG). We also quantified retinal morphology and densities of PSD-95, NMDAR1, CRFR1, and serotonin in the synaptic inner plexiform layer at 7 days, 4 weeks, and 8 weeks of age. Standard RT-PCR and nonsense-mediated decay interference treatment were also performed to assess genetic compensation in mutants.

Results. Relative to wild-type, *pdzk1*-KO larvae showed spatial frequency tuning functions with increased amplitude (likely due to abnormal gain control) and reduced ERG *b*-waves (suggestive of inner retinal dysfunction). No synaptic phenotypes, but possible morphological retinal phenotypes, were identified. We confirmed that the absence of major histological phenotypes was not attributable to genetic compensatory mechanisms.

Conclusions. Our findings point to a role for *pdzk1* in zebrafish visual function, and our model system provides a platform for investigating other genes associated with abnormal visual behavior.

Keywords: PDZK1, visual phenotyping, zebrafish, optomotor response (OMR), electroretinogram (ERG), neurodevelopmental disorders

Altered contrast sensitivity is a visual endophenotype of many neurodevelopmental disorders, including schizophrenia and autism spectrum disorder (ASD).[1,2] A genome-wide association study identified a link between abnormal contrast sensitivity and the single-nucleotide polymorphism (SNP) rs1797052, located in the 5′-untranslated region of the *PDZK1* gene, which is situated in a high-risk locus for schizophrenia and ASD.[3] Variation in this gene may thus contribute to visual deficits observed in a number of different disorders.

As a scaffolding protein, PDZ domain containing 1 (PDZK1) is implicated in neurosynaptic signaling. PDZK1 contains four tandem postsynaptic density 95/disc large/zonula occludens-1 (PDZ) domains,[4] allowing it to interact with proteins possessing PDZ-binding regions. For example, PDZK1 binds with postsynaptic density 95 (PSD-95), *N*-methyl-D-aspartate receptors (NMDARs), synaptic Ras GTPase-activating protein 1 (SynGAP1), and Kelch-like protein 17 (KLHL17) to form a complex that anchors proteins to the cytoskeleton on cell membranes.[5] Like PDZK1, the PSD-95 protein also contains PDZ domains, and functions as a scaffold protein on postsynaptic membranes for excitatory synapses,[6] whereas KLHL17 is a brain-specific Kelch protein that binds to intracellular F-actin, a major component of the cellular cytoskeleton.[7] PDZK1 thus likely plays a role in maintaining the distribution and shape of postsynaptic densities by regulating actin-based neuronal functions.[7] Disruption of PSD-95 (also called DLG4) also affects the neurexin–neuroligin–SHANK pathway, leading to cognitive dysfunction.[8,9]

PDZK1 is important for anchoring and clustering NMDARs, ionotropic glutamate receptors responsible for gating ion influx into neurons.[10] In the visual system, NMDARs regulate contrast gain control, optimizing visual perception of contrast and motion, and abnormalities in these receptors have been hypothesized to underpin visual

disturbances in schizophrenia.[10,11] PDZK1 also regulates signaling and endocytosis for corticotropin-releasing factor receptor 1 (CRFR1) and the serotonin 2A receptor (5-HT2AR).[12] CRFR1 is a vital component of the hypothalamic–pituitary–adrenal axis for stress responses,[13] and it sensitizes serotonin 2 receptors, including 5-HT2AR, to modulate anxiety-related behaviors.[14] PDZK1 thus interacts with multiple membrane-associated proteins for synaptic signaling, with likely impacts on neural processing, visual perception, and behavior. However, despite evidence of genetic associations, to date there has been no direct demonstration of an impact of *PDZK1* disruption on behavior and physiology.

The retina at the back of the eye is an extension of the central nervous system (CNS) that provides a highly accessible readout of gene function in the CNS. Neurodegeneration and neurodevelopmental abnormalities in the brain and spinal cord typically manifest in visual dysfunction, and some CNS disorders (e.g., stroke, multiple sclerosis, Alzheimer's disease) can be diagnosed by ocular symptoms.[15] Compared to the brain, the retina has a relatively straightforward organization with well-characterized excitatory (photoreceptors, bipolar and ganglion cells) and inhibitory (horizontal and amacrine cells) neuronal classes arranged in distinct organized layers. The visual system is highly amenable to assessment, and robust non-invasive behavioral (e.g., optomotor response [OMR]), physiological (e.g., electroretinogram [ERG]), and histological tools allow the neurological function of genes to be comprehensively evaluated across these different phenotypic levels.

The zebrafish (*Danio rerio*) has key advantages as a model for studying both visual and gene function, including conserved retinal architecture and genetics with other vertebrates, ease of genetic manipulation, high fecundity, and rapid development. Importantly, as in humans, a single *pdzk1* gene is expressed in larval zebrafish retina and brain.[16] Here, we characterized the effects of *pdzk1* disruption using clustered regularly interspaced short palindromic repeats (CRISPR)/CRISPR-associated protein 9 (Cas9) genome modification to generate a *pdzk1* knockout (*pdzk1*-KO) zebrafish mutant. Visual behavior was assessed by quantifying spatial frequency tuning and contrast response functions using OMR, and the physiological function of the retina was examined with ERG. To investigate possible histological correlates of the observed behavioral and functional phenotypes, we quantified general retinal morphology via retinal size and thickness of the whole retina or synaptic inner plexiform layer (IPL), as well as the density of PSD-95, NMDAR1, CRFR1, and serotonin in the IPL. Our results suggest that, relative to wild-type larvae, *pdzk1*-KO larvae show abnormal contrast gain control, with significantly lower contrast thresholds that likely cause an increase in the overall amplitude of the spatial frequency tuning function. In addition, *pdzk1*-KO larvae showed clear deficits in retinal function, with a reduction in the ERG *b*-wave amplitude suggesting dysfunction of the inner retina. We found no clear differences between *pdzk1*-KO and wild-type fish in anatomical and histological markers at 7 days post-fertilization (dpf), 4 weeks post-fertilization (wpf), and 8 wpf, ruling out a number of the most likely candidates for the anatomical substrate underlying the effects of *pdzk1* on visual function.

Methods

Data Availability

Data for the present study are available on the Open Science Framework (https://osf.io/s49z6).

Animal Husbandry

Zebrafish *(Danio rerio)* were maintained and bred in the Fish Facility at the Walter and Eliza Hall Institute of Medical Research according to local animal guidelines. For experiments at 7 dpf, embryos and larvae (prior to sex determination) were grown in Petri dishes in an incubator at 28.5°C before use. Fish for experiments at higher ages were grown in Petri dishes at 28.5°C up to 5 dpf, then introduced to tanks and raised in flow-through systems at 28°C. All procedures were approved by the Faculty of Science Animal Ethics Committee at the University of Melbourne (Project No. 1614017.3) and adhered to the ARVO Statement for the Use of Animals in Ophthalmic and Vision Research.

Generation of Mutants

To disable *pdzk1* gene function, we applied a CRISPR/Cas9 system according to published protocols.[17] The guide RNA (Table), Cas9 enzyme (Genesearch, Arundel, Australia), and stop-codon cassette (Table) with homologous sequence hands were co-injected into zebrafish zygotes. Homology-directed repair resulted in a premature stop codon at exon 2 of the *pdzk1* gene, leading to the loss of functional Pdzk1 in mutants (Figs. 1a–a″). To highlight retinal cell layers for quantification of retinal morphology, the Tg(*ptf1a*:*GFP*) line was crossed with the *pdzk1*-KO mutants to generate a *pdzk1*-KO/Tg(*ptf1a*:*GFP*) line, in which the retinal horizontal and all amacrine cells were labeled by green fluorescent proteins.[18,19] The mutants used in this study were all homozygous *pdzk1*-KO zebrafish, including those expressing the Tg(*ptf1a*:*GFP*) construct.

Genotyping

For DNA isolation, small wedges of fin were cut from anesthetized 3-month-old fish. Fin samples were incubated in lysis buffer (10-mM Tris-HCl, 50-mM KCl, 0.3% Tween, and 0.3% IGEPAL, pH 8.3; Rhodia, Paris, France) with 1.25-mg/mL Proteinase K (03115879001; Roche Australia, Bella Vista, NSW, Australia) at 55°C for 2.5 hours, followed by incubation at 98°C for 10 minutes. Isolated DNA was used as a template for PCR amplification of the targeted *pdzk1* genomic DNA sequence (genomic DNA primers) (Table). The PCR program was comprised of an initial denaturation step of 98°C for 3 minutes, 35 cycles of 98°C for 30 seconds, 60°C for 30 seconds, and 72°C for 1 minute, followed by a final extension step of 72°C for 3 minutes. Electrophoresis of the PCR products was performed using 3% Tris-acetate-EDTA (TAE) agarose gel. Target bands were cut from electrophoresis gels, and the PCR products were extracted using a QIAquick Gel Extraction Kit (QIAGEN, Hilden, Germany). Extracted products were amplified by PCR using a forward primer (primer for sequencing) (Table) and sent to Macrogen (Seoul, South Korea) for sequencing.

Investigative Ophthalmology & Visual Science

Table. Oligonucleotides

Oligonucleotides for CRISPR (5′–3′)		
Guide RNA (gRNA)	GAAGGTAGAAGCCATAACCC + short hairpin RNA scaffold	
Stop-codon cassette sequence	5′ homologous hands + GTCATGGCGTTTAAACCTTAATTAAGCTGTTGTAG + 3′ homologous hands	
Primer Pairs	**Forward (5′–3′)**	**Reverse (5′–3′)**
Genomic DNA primers	AGTTTCAGTGTGTTTGTGTTGCA	CACCTAAAGTGTGCACTGTGT
Primer for sequencing	GCTGGGGAAAATACTTTCAGACA	
P1	CAACAGACACCTCCTTTACAACA	CACCAGGAGGCAGCATTT
P2	TAAACCTTAATTAAGCTGTTGTAGT	CACCAGGAGGCAGCATTT

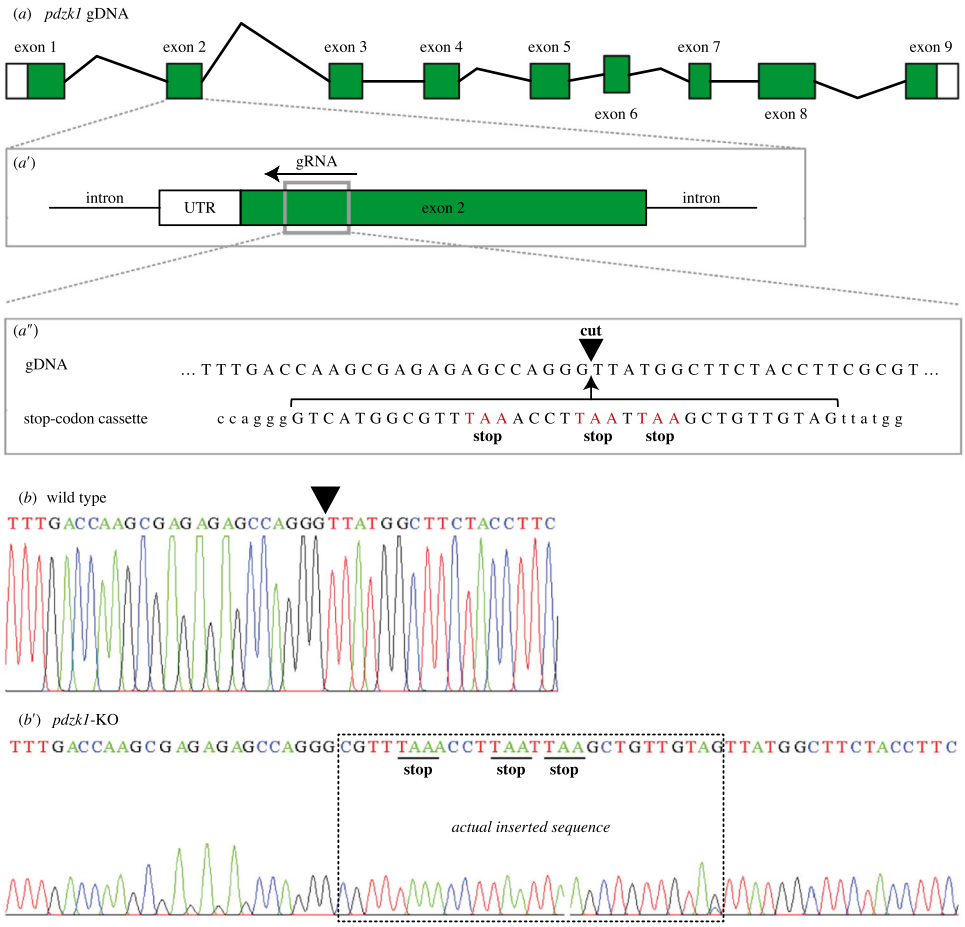

Figure 1. CRISPR editing of *pdzk1*. (**a**) There are nine exons in *pdzk1* genomic DNA. (**a′**) The guide RNA (gRNA) targets a site in exon 2 (*gray box*) and recruits the Cas9 enzyme to recognize and cut the DNA. (**a″**) The target cut site (*black inverted triangle*) has homologous arms matching the stop codon template that is co-injected with Cas9 and gRNA during the one-cell stage of zebrafish development. In this way, homology-directed repair inserts the stop codon cassette at exon 2 of *pdzk1*. Stop codons of the injected cassette are highlighted in *red*. (**b**) Sequence results for wild-type fish. The inverted triangle indicates the targeted cut site. (**b′**) Sequence results for homozygous *pdzk1*-knockout fish. The box shows the sequence inserted by CRISPR gene editing including the three stop codons (*underlined*). Sequences on either side were identical to the wild-type fish.

Optomotor Response

Apparatus and Procedure. The OMR apparatus was adapted from one previously described (Supplementary Fig. S1; Supplementary Methods).[20,21] Groups of 7-dpf larvae of a single genotype (between 50 and 58 larvae in each group) were contained in a six-lane arena with a transparent base (one group per lane) (Supplementary Fig. S1b). During a trial, a test stimulus was displayed on a screen below the arena, drifting at 25°/s, 50°/s, or 100°/s parallel to the long axis of the lanes (Supplementary Fig. S1a). Prior to each trial, a corralling stimulus (25°/s drift) was shown for 30 seconds to guide larvae to the center of the lane (Supplementary Fig. S1d). This was followed by a 30-second presentation of a test stimulus, with a webcam capturing digital images before and after each presentation. A blank gray screen was presented after the offset of the test stimulus as the texture for the next trial was computed.

For measurement of spatial frequency tuning functions, test stimuli were Gaussian noise textures, filtered to be spatial frequency bandpass with center frequencies of 0.005, 0.01, 0.02, 0.04, 0.08, 0.16, or 0.32 cycle per degree (cpd) (SD = 0.5 octaves) at full contrast (100%). For measurement of contrast response functions, the center spatial frequency was 0.02 cpd (SD = 0.5 octaves), with textures presented at 1%, 3%, 5%, 10%, 30%, 50%, or 100% contrast.

Before experiments, larvae were transferred to arena lanes within 10 minutes, after which they were allowed to adapt to the arena for 10 minutes. All experiments were conducted between 9:30 AM and 6:00 PM. After experiments, larvae were humanely killed using 0.1% tricaine (E10521-50G; Sigma-Aldrich, St. Louis, MO, USA).

OMR Image Analysis. Larval positions were extracted from before and after images for each trial. Within each lane, the change in position of the group centroid (i.e., average position of the group) in the direction of texture motion was computed as the optomotor index (OMI) (see Supplementary Methods). Normalized OMIs for spatial frequency tuning functions were calculated by normalizing all data to the OMI of wild-type larvae for 100%-contrast, 0.02-cpd stimuli drifting at 25°/s (i.e., the condition typically producing the greatest response). The spatial frequency tuning function was fitted as a log-Gaussian using a least-squares criterion. For each fitted model, the estimated parameters were

Investigative Ophthalmology & Visual Science

amplitude (i.e., height of the peak), peak spatial frequency (i.e., spatial frequency at which amplitude peaked), and bandwidth (i.e., standard deviation). There were 72 trials for each genotype (*pdzk1*-KO and wild-type), per combination of spatial frequency and speed (i.e., 1512 trials per genotype in total across all conditions). Normalized OMIs for contrast response functions were calculated by normalizing all data to the OMI of the wild-type group for 100% contrast at 50°/s and 0.02 cpd. The contrast response function was fitted as a two-parameter piecewise function (Equation 1) using a least-squares criterion:

$$y = \begin{cases} 0, & x < k \\ (x-k)^a, & x \geq k \end{cases} \quad (1)$$

where y is the OMI, x is log stimulus contrast, k is the contrast threshold (i.e., minimum contrast to evoke an optomotor response), and a is response gain (i.e., slope of the function). There were 36 trials for wild-type and 24 trials for mutants, per combination of contrast and speed (i.e., 756 trials for wild-type and 504 trials for mutants in total across all conditions).

To test whether spatial frequency tuning and contrast response functions differed between groups, an omnibus F test was used to compare the goodness of fit (r^2) of a full model, in which parameter estimates of each group could vary independently, with that of a restricted model, in which parameters were constrained to be the same across groups. To determine whether specific parameter estimates differed between groups, a nested F test was used to compare a full model with a restricted model in which one parameter was constrained to be the same across groups.[22] A criterion of $\alpha = 0.05$ was used to determine significance, with Bonferroni correction applied to P values to account for multiple testing where appropriate.

Locomotor Response

Locomotion assays were performed on 7-dpf zebrafish according to a previously published protocol.[23] Prior to testing, zebrafish were either treated with 1.5% ethanol in embryo medium (E3) or left in standard E3 medium for 10 minutes. Embryos were plated into 24-well dishes in a pseudorandom order, with the experimenter blinded to genotype during testing and data analysis. An inactivity threshold of 1 mm/s, a detection threshold of 25 mm/s, and a maximum burst threshold of 30 mm/s were applied. For the 10-minute test period in dark, the total distance swum and the swimming speed above inactivity threshold and below maximum burst threshold were extracted using ZebraLab software (Viewpoint Life Sciences, Lyon, France). Indicators of normality were derived from D'Agnostino and Perron's test; outliers were identified using the ROUT method and excluded from analysis. Two-way ANOVA (genotype × treatment) with Bonferroni correction was performed in Prism 7 (GraphPad, San Diego, CA, USA) ($\alpha = 0.05$). There were between 106 and 108 larvae for the analysis of swimming distance, and between 103 and 106 larvae for the analysis of swimming speed, per combination of genotype and treatment (see Supplementary Table S1).

Electroretinography

Scotopic ERGs were measured in 7-dpf fish according to our published method.[24] Larvae were dark adapted (>8 hours, overnight) prior to experiments and anesthetized using 0.02% tricaine in 1× goldfish Ringer's buffer. For testing, an individual larva was transferred onto a moist polyvinyl alcohol (PVA) sponge platform. Under dim red illumination (17.4 c·d·m^{-2}; λ_{max} = 600 nm), a sponge-tipped recording electrode (<40-µm diameter) gently touched the central corneal surface of the larval eye, and the reference electrode was inserted into the sponge platform. After electrode placement, the platform was inserted into a Ganzfeld bowl, and the larva was allowed to dark adapt for >3 minutes. ERG responses were recorded from 22 wild-type and 26 *pdzk1*-KO larvae with flash stimuli at −2.11, −0.81, 0.72, 1.89, or 2.48 log cd·s·m^{-2}. At −2.11 and −0.81 log cd·s·m^{-2}, three repeats were measured with an inter-flash interval of 10 seconds. At 0.72 to 2.48 log cd·s·m^{-2}, a single response was measured with 60 seconds between flashes. All experiments were performed between 9:00 AM and 6:00 PM at room temperature. Larvae were humanely killed after experiments using 0.1% tricaine. Amplitudes of the *a*- and *b*-waves were measured from baseline to the negative *a*-wave trough and from the negative *a*-wave trough to the *b*-wave peak, respectively. Implicit times of the *a*- and *b*-waves were measured from stimulus onset to the *a*-wave trough and the *b*-wave peak, respectively. Two-way ANOVA with Bonferroni correction was performed in Prism 7 ($\alpha = 0.05$).

Histology

Immunohistochemistry. Whole zebrafish at 7 dpf or 4 wpf, or dissected zebrafish eyes at 8 wpf, were fixed in 4% paraformaldehyde (PFA) in PBS for 3 hours at room temperature, or overnight at 4°C. They were cryoprotected in 30% sucrose in PBS, embedded in Tissue-Tek OCT compound, and cryosectioned (12 µm; CM 1860 Cryostat; Leica, Wetzlar, Germany). For wild-type and *pdzk1*-KO larvae, antibody staining was carried out at room temperature using standard protocols. Antigen retrieval was performed by incubating slides in boiled 10-mM sodium citrate (pH 6) until the solution was cooled to room temperature. Slides were blocked in 5% fetal bovine serum (FBS) for 30 minutes and incubated overnight in rabbit anti-PSD-95 (ab18258, 1:100; Abcam, Cambridge, UK), anti-CRFR1 (ab59023, 1:100; Abcam), anti-GluN1 (to label an NMDA receptor subunit; 114 011, 1:400; Synaptic Systems, Goettingen, Germany), or anti-serotonin (ab66047, 1:500; Abcam) primary antibodies diluted in FBS. Slides were subsequently incubated for 2 hours in secondary antibodies (all 1:500; Thermo Fisher Scientific, Waltham, MA, USA) diluted in 5% FBS. The secondary antibodies used were Goat anti-Rabbit Alexa Fluor 488 (A11008) or Alexa Fluor 546 (A11010), Goat anti-Mouse Alexa Fluor 488 (A11001), and Donkey anti-Goat Alexa Fluor 488 (A11055). Nuclei were counterstained with 4′,6-diamidino-2-phenylindole (DAPI; D9542-10MG, 1:10000; Sigma-Aldrich) in PBS for 20 minutes, and sections were mounted in Mowiol (81381-250G; Sigma-Aldrich). For Tg(*ptf1a*:*GFP*) and *pdzk1*-KO/Tg(*ptf1a*:*GFP*) larvae, samples were stained with DAPI only, following cryostat sectioning.

Retinal Image Acquisition. For quantification of IPL densities, retinas stained with antibodies for PSD-95, NMDAR1, CRFR1, and serotonin from *pdzk1*-KO and wild-type larvae were imaged using a Nikon A1R confocal microscope (Nikon, Tokyo, Japan) with a 60× or 40× oil objective lens. For quantification of IPL thickness, retinal size and retinal thickness, images of retinal sections of Tg(*ptf1a*:*GFP*) and *pdzk1*-KO/Tg(*ptf1a*:*GFP*) larvae were taken within two

Investigative Ophthalmology & Visual Science

sections from the optic nerve, using a Zeiss Axioscope (Carl Zeiss Microscopy, Oberkochen, Germany) with a 20× objective lens, or a Nikon A1R confocal microscope with a 40× oil objective lens. For all confocal imaging, the deconvolution function was applied to minimize background noise.

Retinal Image Analysis. To measure puncta density, three regions of interest (ROIs; 10 × 20 µm) were randomly selected from the IPL of one confocal image for each retina using FIJI, a distribution of ImageJ (National Institutes of Health, Bethesda, MD, USA).[25] For each ROI, thresholding was performed with the Invert lookup table (LUT) function to select areas containing no puncta and create a background mask. All potential puncta in the ROI were identified as dots using the Find Maxima function. Dots identified in the background area (i.e., noise) were masked using the Image Calculator function and the background mask. The remaining dots in the ROI were considered true puncta and quantified for analysis. The density of the analyzed molecule in each retinal image was quantified as the average of three ROIs. Statistical analysis for puncta density was performed using two-way ANOVA with Bonferroni correction (Prism 7; $\alpha = 0.05$). To quantify evidence for null hypotheses, we also calculated Bayesian ANOVA using JASP ($BF_{inclusion} = 0.33$, meaning the data are at least three times as likely under the null hypothesis than the alternative).[26]

Images of Tg(*ptf1a*:*GFP*) and *pdzk1*-KO/Tg(*ptf1a*:*GFP*) retinal sections were used for analysis of retinal size, IPL thickness, retinal thickness, retinal length, and amacrine cell number using FIJI. Tg(*ptf1a*:*GFP*) clearly labels all developing inhibitory neurons (horizontal and amacrine interneurons) in the retina throughout the early larval stage.[19] Although ptf1a expression itself is transient, we have observed green fluorescent protein (GFP) labeling to be stable up 10 to 12 dpf. The lamination of the retina allows us to clearly distinguish between horizontal cells, situated in the outermost division of the inner nuclear layer, and amacrine cells, situated in the inner division of the inner nuclear layer. These divisions are separated in zebrafish retina by three unlabeled cell layers containing bipolar interneurons and Müller glia. For retinal size, the polygon selection function was used to outline the whole retinal section around the outer segments of the photoreceptors, around the ciliary margin, and along the nerve fiber layer adjacent to the lens (Supplementary Fig. S2a). IPL thickness was measured by a masked observer in three locations (central and 45° on either side) (Supplementary Fig. S2a). For each eye, the average over the three locations was taken as the IPL thickness. Similarly, retinal thickness was measured as the average retinal thickness in the three locations in the same samples (Supplementary Fig. S2a) but using the DAPI staining to accurately identify the outermost photoreceptor boundary and innermost nerve fiber boundary. Retinal length was measured as the length from one end of the retina around the ciliary margin, along the middle layer of the IPL, to the ciliary margin at the other retinal end (Supplementary Fig. S2a). For statistical analysis, retinal size, IPL thickness, retinal thickness, and retinal length were normalized to the mean of wild-type group parameters. To determine the number of amacrine neurons, we manually counted ptf1a-positive (ptf1a+) cells indicated by GFP+ cell bodies in the inner half of the inner nuclear layer and the ganglion cell layer of whole retinal sections (Supplementary Fig. S2b). These counts were standardized to the average length of wild-type retinas (520.0 µm from 12 retinal sections). Morphological distributions were approximately normal and were analyzed using unpaired *t*-tests (Prism 7; $\alpha = 0.05$). There were between 12 and 31 retinas per group for puncta density analysis (Supplementary Table S2), and 12 (wild-type) or 13 (*pdzk1*-KO) retinas for morphological analysis.

Genetic Compensation Test

Standard RT-PCR. To confirm that the *pdzk1* gene has no functional splice variants except for that targeted by our CRISPR for insertion of the stop-codon cassette, we used standard RT-PCR. Twenty larvae per genotype were used for RNA extraction using the QIAGEN RNeasy Mini Kit. Copy DNA was generated by reverse transcription using a Tetro cDNA synthesis kit (Bioline, London, UK). The zebrafish *pdzk1* gene has nine exons. Primers were designed against (i) an RNA region across exons 1 to 6 containing the insertion site (primer pair 1 [P1]) and (ii) a region starting with the stop-codon cassette insertion in exon 2 and ending in exon 6 (primer pair 2 [P2]) (Table; see Fig. 7a). PCR conditions were 98°C for 3 minutes (one cycle), 98°C for 30°seconds, 56°C for 30 seconds, 72°C for 1 minute (35 cycles), and 72°C for 3 minutes. Electrophoresis was performed using 3% TAE agarose gel, and products were imaged under ultraviolet light.

Nonsense-Mediated Decay Interference Treatment. *pdzk1*-KO embryos were randomly assigned to two groups after collection. From 3 dpf, the two groups were immersed in either 0.02% dimethyl sulfoxide (DMSO) or 10-µM NMDi14 (SML1538; Sigma-Aldrich)/0.02% DMSO dissolved in egg water (60 mg/L sea salt), as control or experimental groups, respectively.[27] NMDi14 is a drug for blocking nonsense-mediated decay of mutant mRNA, which is a trigger for genetic compensation. At 7 dpf, the two groups were assessed by OMR, ERG, and histology, as described above. Statistical analysis was performed using *F* tests (a custom MATLAB algorithm; MathWorks, Natick, MA, USA), two-way ANOVA with Bonferroni correction, and unpaired *t* tests (Prism 7; $\alpha = 0.05$). Sample size for each experiment is detailed in Supplementary Table S6.

Results

Mutant Generation

We used CRISPR/Cas9 to generate the *pdzk1*-KO mutant (Figs. 1a–a″). DNA sequencing from wild-type and homozygous *pdzk1*-KO fish showed that, in mutants, the stop codon cassette was successfully inserted into the target site of the zebrafish *pdzk1* genomic DNA (gDNA) (Figs. 1b, b′), resulting in a mutated *pdzk1* gDNA. By observation, *pdzk1*-KO mutants look grossly equivalent to wild-type fish throughout all developmental stages in morphology and prey and schooling behaviors, although more detailed analysis was not conducted. Visual inspection of swimming behavior revealed no gross abnormalities for *pdzk1*-KO larvae. The knockout mutant was fertile and survived well into adulthood.

Spatial Frequency Tuning Functions

To determine the contribution of *pdzk1* to spatial vision, we measured the spatial frequency tuning function using OMR in 7 dpf wild-type and *pdzk1*-KO larvae. All spatial frequency tuning functions were well fit by a log-Gaussian model (Figs. 2a–c). In an omnibus test (Supplementary Table S3),

Investigative Ophthalmology & Visual Science

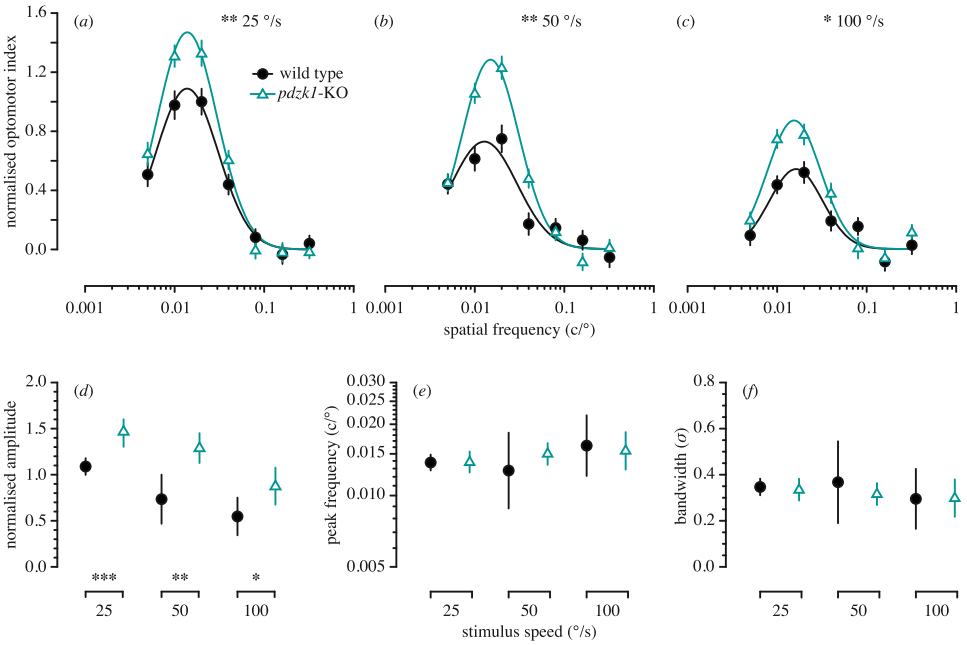

Figure 2. Spatial frequency tuning functions measured using the OMR of wild-type and *pdzk1*-KO larvae. The *upper panels* show normalized optomotor index as a function of spatial frequency for wild-type (*black circles* and *lines*) and *pdzk1*-KO larvae (*cyan triangles* and *lines*) at (**a**) 25°/s, (**b**) 50°/s, and (**c**) 100°/s. Spatial frequency tuning functions are three-parameter log-Gaussian functions fit to the data by minimizing the least-squares error. *Error bars* show ± SEM across trials. The *bottom panels* show (**d**) normalized amplitude, (**e**) peak spatial frequency, and (**f**) bandwidth as a function of group at the three stimulus speeds tested. *Error bars* show 95% confidence intervals on the fitted parameter. *$P < 0.05$; **$P < 0.01$; ***$P < 0.001$ for the omnibus comparison of functions (*upper panels*) and for the comparison of individual parameters (*lower panels*) between genotypes.

overall spatial frequency tuning functions statistically differed between wild-type and *pdzk1*-KO larvae at each speed (Figs. 2a–c). Examining individual parameters, there was a significantly higher amplitude (i.e., height of the spatial frequency tuning function peak) (Fig. 2d; Supplementary Table S3) for mutants compared with wild-type fish at each speed tested. No differences were found in the peak frequency (Fig. 2e) or bandwidth (standard deviation; Fig. 2f) of the tuning function at any speed (Supplementary Table S3).

Contrast Response Functions. To examine whether the increased amplitude of the spatial frequency tuning function in *pdzk1*-KO mutants was due to altered contrast gain (i.e., decreased threshold) or response gain (i.e., increased motor response to suprathreshold stimuli), we used OMR to measure the contrast response function at 0.02 cpd, at which zebrafish larvae typically showed the most robust responses. Contrast response functions were well fit by a two-parameter piecewise function (Fig. 3). In omnibus analysis, functions were significantly different between groups at 25°/s, 50°/s, and 100°/s ($P < 0.001$, $P = 0.006$, and P = 0.01, respectively) (Figs. 3a–c; Supplementary Table S4). Examining individual parameters, we found no difference in response gain (function slope) between wild-type and mutant groups at any tested speed (Fig. 3d; Supplementary Table S4). However, the contrast threshold was significantly lower for mutants than for wild-type larvae at 25°/s and 50°/s ($P < 0.001$ and $P = 0.002$, respectively) (Fig. 3e; Supplementary Table S4), indicating a higher contrast sensitivity for mutants. Overall, all OMR contrast response functions deviated upward at lower contrasts for mutants than for wild-type larvae, suggesting that the augmented spatial frequency tuning functions in mutants reflect increased contrast gain rather than response gain.

To further examine the possibility that increased locomotion, rather than increased visual sensitivity, was the cause of the augmented *pdzk1*-KO optomotor response, we conducted a locomotor assay. Prior to measurement, larvae were either untreated or exposed to 1.5% ethanol to stimulate a hyperactive phenotype.[28] As expected, ethanol exposure increased activity in both wild-type ($P < 0.0001$ for both swimming distance and speed) and *pdzk1*-KO larvae ($P < 0.0001$ for both swimming distance and speed) (Supplementary Fig. S3, Supplementary Table S1). However, both with and without stimulation, mutants swam significantly shorter distances (both $P < 0.0001$) and at slower speeds ($P < 0.0001$ and $P = 0.003$ for untreated and treated, respectively) than wild-type larvae. That the OMR is augmented in *pdzk1*-KO fish despite reduced spontaneous and ethanol-induced locomotion suggests it is indeed driven by improved contrast sensitivity.

Electroretinography

We conducted scotopic ERG measurements for wild-type controls and mutant larvae. Compared to wild-type, *pdzk1*-KO showed significantly smaller *b*-wave amplitudes ($P < 0.0001$), particularly at higher stimulus intensities ($P = 0.03$ and $P < 0.0001$ for 1.89 and 2.48 log cd·s·m^{-2}, respectively) (Figs. 4a, d; Supplementary Table S5). There were no statistical differences in *a*-wave amplitudes nor in implicit times of *a*- and *b*-waves between wild-type and *pdzk1*-KO mutants (Figs. 4a–c, e; Supplementary Table S5).

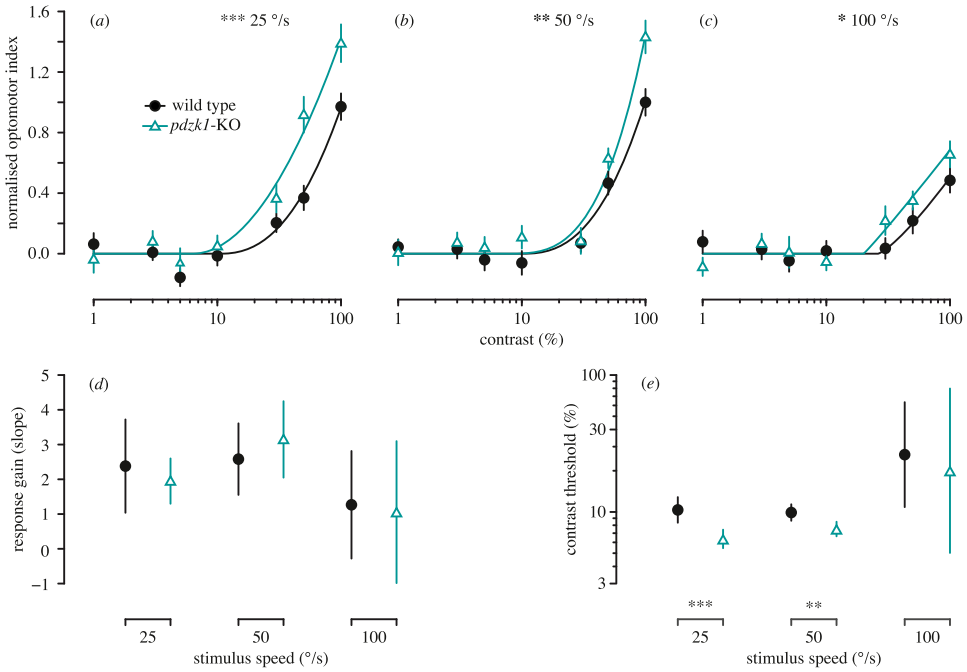

Figure 3. Contrast response functions measured using the OMR in wild-type (*black circles* and *lines*) and *pdzk1*-KO larvae (*cyan triangles* and *lines*) at (**a**) 25°/s, (**b**) 50°/s, and (**c**) 100°/s. Contrast response curves are fit to the data using two-parameter piecewise functions by minimizing the least-squares error with respect to the data. *Error bars* show ±SEM across trials. The bottom panels show (**d**) response gain and (**e**) contrast threshold as a function of group at the three stimulus speeds tested. *Error bars* show 95% confidence intervals on the fitted parameter. *$P < 0.05$; **$P < 0.01$; ***$P < 0.001$ for the omnibus comparison of functions (*upper panels*) and for the comparison of individual parameters (*lower panels*) between genotypes.

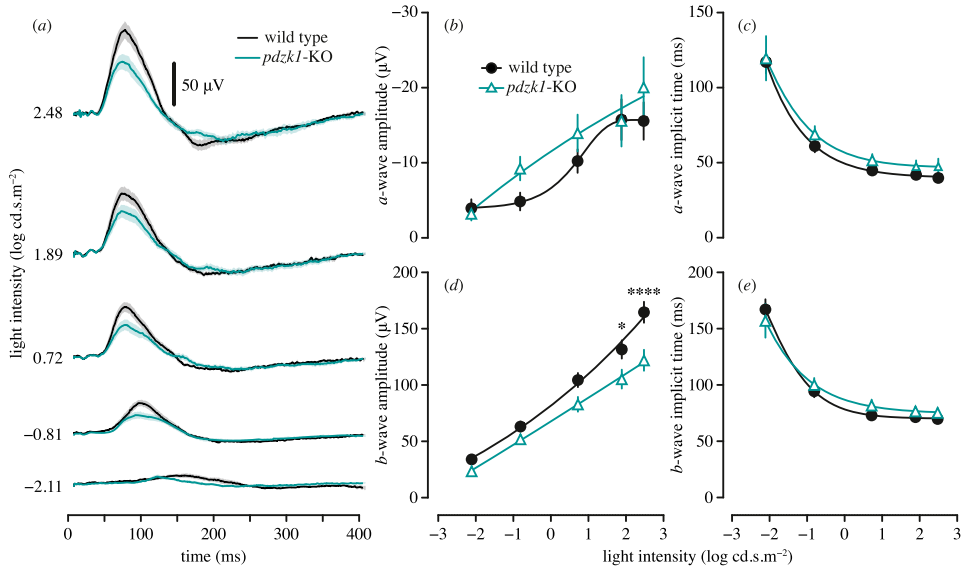

Figure 4. Scotopic ERGs of wild-type and *pdzk1*-KO larvae. (**a**) Group average ERG traces. Wild-type and *pdzk1*-KO larvae responses are shown as *black* and *cyan lines*, respectively, at −2.11, −0.81, 0.72, 1.89, and 2.48 log cd·s·m^{-2}. *Scale bar*: 50 µV. The light bands around group average traces represent ±1 SEM. Note that the *a*-wave is not visible in the group averages owing to variability in the implicit time, which causes the individual traces to cancel out. Remaining panels show group average (±SEM) (**b**) *a*-wave amplitude, (**c**) *a*-wave implicit time, (**d**) *b*-wave amplitude, and (**e**) *b*-wave implicit time for wild-type (*black circles*) and *pdzk1*-KO (*cyan triangles*) larvae. Lines were fit using a four-parameter sigmoidal function. Data were compared using two-way ANOVA with Bonferroni correction. *$P < 0.05$; ****$P < 0.0001$.

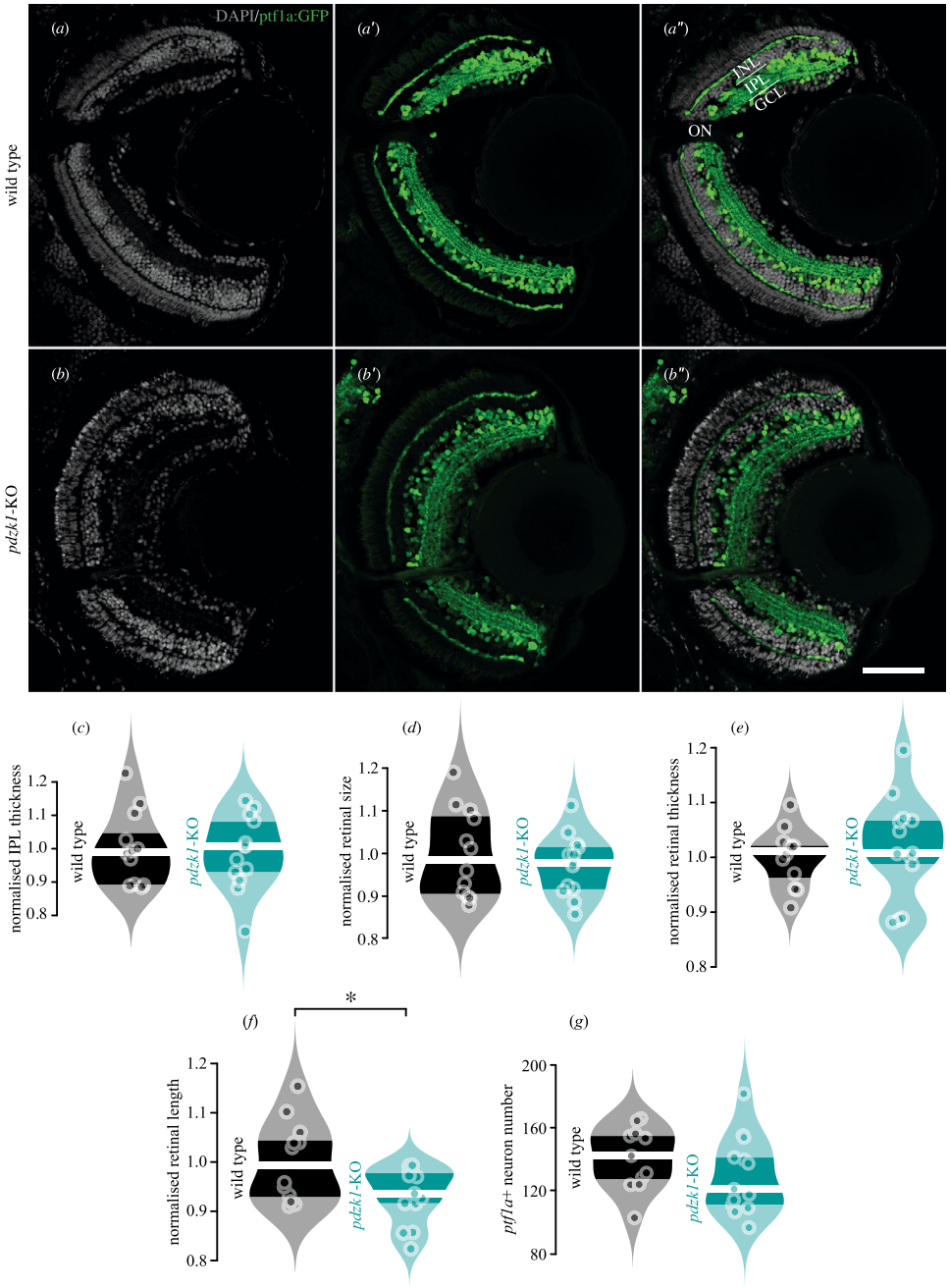

Figure 5. Transgenic labeling of retinal layers and quantification of retinal morphology for wild-type and *pdzk1*-KO larvae. (**a–b″**) Inhibitory neurons, including horizontal and amacrine cells, and their projections into the outer and inner plexiform layers were labeled by transgenic construct Tg(*ptf1a*:*GFP*) in *green*, revealing distinct retinal layers in wild-type and *pdzk1*-KO retinas. Nuclei stained with DAPI are shown in *gray*. *Scale bar*: 50 µm. Normalized (**c**) IPL thickness, (**d**) retinal size, (**e**) retinal thickness, (**f**) retinal length, and (**g**) *ptf1a* positive (*ptf1a*+) neuron number were quantified. Points are data from individual retinas. *White lines* represent medians, and *dark bands* indicate interquartile ranges. For all analyses, unpaired *t*-tests were performed with 12 and 13 retinas for wild-type and *pdzk1*-KO groups, respectively. $^*P < 0.05$. INL, inner nuclear layer; IPL, inner plexiform layer; GCL, ganglion cell layer; ON, optic nerve.

Retinal Morphology

Differences in retinal function might arise from changes to retinal morphology. To identify distinct layers in the zebrafish retina, we used the transgenic construct Tg(*ptf1a*:*GFP*) to genetically label horizontal and amacrine cells and their projections into the outer plexiform layer (OPL) and IPL, respectively (Figs. 5a–b″). Our quantification revealed no difference in IPL thickness, retinal size, retinal thickness, or amacrine (*ptf1a*+) cell number in *pdzk1*-KO compared with wild-type larvae (Figs. 5c–e, g; Supplementary Fig. S2; Supplementary Table S6). We found a significant

Investigative Ophthalmology & Visual Science

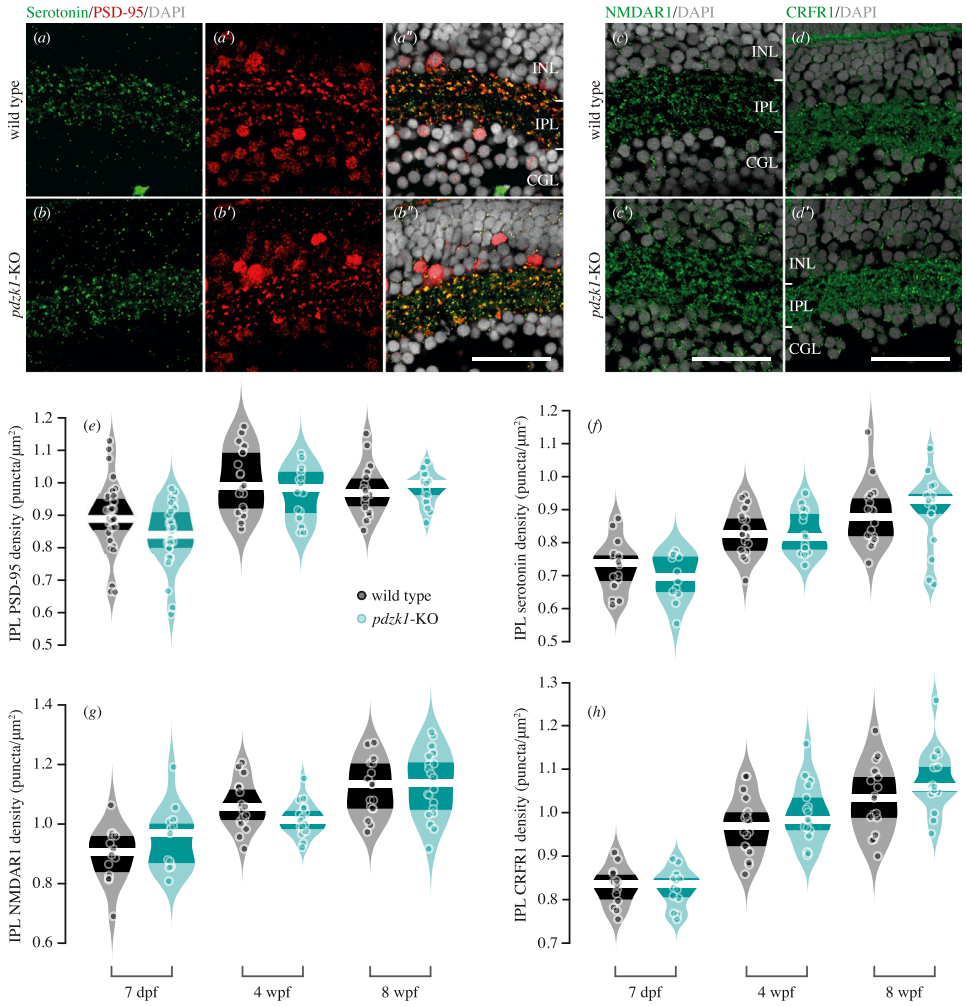

Figure 6. Immunostaining and density quantification of PDZK1-interacting molecules in wild-type and *pdzk1*-KO retinas. Micrographs of retinal sections from 7-dpf wild-type and *pdzk1*-KO larvae were co-labeled with (**a–b″**) serotonin and PSD-95 in *green* and *red*, respectively. (**c**, **c′**) NMDAR1 and (**d**, **d′**) CRFR1 were labeled in *green* for 7-dpf retinas. For all images, nuclei were stained with DAPI, shown in *gray*. *Scale bars*: 25 µm. Violin plots show densities of (**e**) PSD-95, (**f**) serotonin, (**g**) NMDAR1, and (**h**) CRFR1 in the IPL at 7 dpf, 4 wpf, and 8 wpf. Points are data from individual retinas. *White lines* represent medians, and *dark bands* indicate interquartile ranges. Statistical comparisons were performed using two-way ANOVA with Bonferroni correction and Bayesian ANOVA. There were between 12 and 31 retinas per group (see Supplementary information). $BF_{inclusion} < 0.33$ was considered to be evidence for the null hypothesis (i.e., the data are at least three times as likely under the null hypothesis than the alternative).

reduction in retinal length for the mutants' relative wild-type larvae ($P = 0.02$) (Fig. 5f), although overall retinal organization seemed normal.

PSD-95, Serotonin, NMDAR1, and CRFR1 Density in the Retinal IPL

To investigate potential subcellular mechanisms underlying the observed changes in visual function, we quantified the density of synaptic signaling molecules known to interact with PDZK1 (i.e., PSD-95, serotonin, NMDAR1, and CRFR1) in the IPL at 7 dpf, 4 wpf, and 8 wpf. As there is no commercially available antibody for the serotonin 2A receptor, we labeled serotonin to assess the effect of *pdzk1* knockout on the serotonin system. Interestingly, in both wild-type and *pdzk1*-KO larvae, our serotonin antibody rarely labeled serotonin in cell bodies, but there was strong serotonin co-labeling with PSD-95 on cell membranes and in synapses (Figs. 6a–b″; Supplementary Figs. S4a–d″).

The four molecules were labeled throughout the retina, but no difference was observed between wild-type and *pdzk1*-KO fish at the ages assessed (Figs. 6a–d′; Supplementary Fig. S4). Similarly, two-way ANOVA of puncta density in IPL did not reveal any differences among the groups (Figs. 6e–h; Supplementary Table S1). Bayesian ANOVA[26] provided support for the null hypothesis of no difference for serotonin and NMDAR1 puncta densities across all tested ages ($BF_{inclusion} = 0.18$ and $BF_{inclusion} = 0.26$, respectively) (Figs. 6f, g; Supplementary Table S2), suggesting these two molecules are particularly unlikely to underlie the altered retinal function.

Genetic Compensation Test

Previous studies have reported that alternative splicing of the mutated mRNA frequently occurs in CRISPR-generated mutants by skipping the whole exon of the target locus, which may result in the production of functional or partially

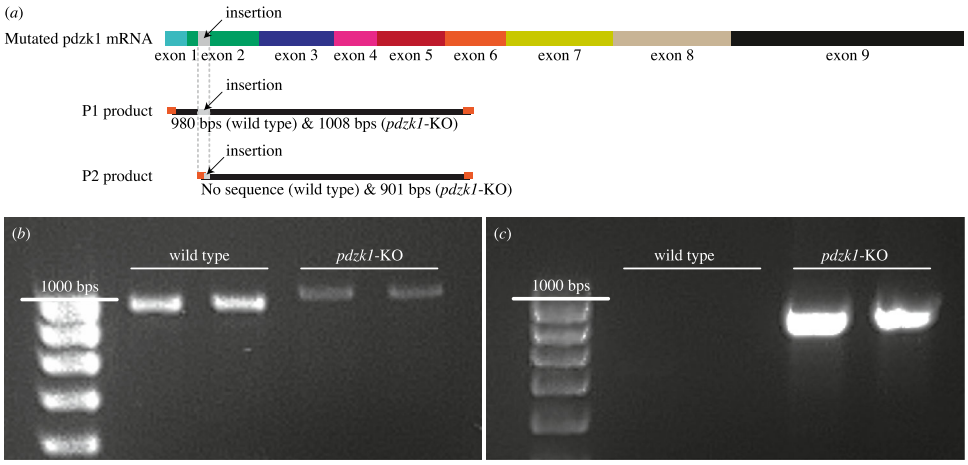

Figure 7. Standard RT-PCR for testing splice variants, exon skipping, and expression of *pdzk1* in wild-type fish and *pdzk1*-KO mutants. (**a**) Schematics of the two primer pairs for *pdzk1* mRNA and their products. Pdzk1 mRNA is expressed from the nine exons of *pdzk1* genomic DNA. In mutants, the insertion (highlighted in *gray* on the *pdzk1* mRNA sequence and primer products) should also be expressed within the exon 2 region (*green*) of the mRNA. Primer pair 1 (P1) was designed to amplify the mRNA region across exons 1 to 6 containing the insertion, producing 980-bp products for wild-type fish and longer (1008-bp) products for mutants due to the insertion. Primer pair 2 (P2) was designed to amplify the mutated *pdzk1* mRNA sequence, which starts within the insertion in exon 2 and ends in exon 6. P2 produces 901-bp products only for mutants, with no product for wild-type controls. *Orange ends* of products represent primers. (**b**) As expected, standard RT-PCR using P1 produced slightly longer products for mutants than for wild-type fish. (**c**) RT-PCR using P2 produced ~900-bp products for mutants but no amplified sequence for wild-type fish.

functional proteins.[29,30] In addition, mutant mRNA degradation due to nonsense-mediated decay (NMD) can activate compensatory genetic mechanisms, leading to transcriptional adaptation in genetically modified models.[27] These mechanisms may rescue the loss of the target gene function, leading to false-negative results in phenotyping. The *pdzk1*-KO larvae in the present study presented significant changes in visual behavior (OMR) and retinal function (ERG) relative to wild-type larvae, but only minor changes in retinal morphology and normal synaptic molecular density. Thus, we conducted genetic compensation tests to uncover potential genetic mechanisms that may have masked histological deficits.

Using standard RT-PCR, we showed a longer mutant *pdzk1* mRNA sequence compared to wild-type mRNA, due to insertion of the stop-codon cassette (Figs. 7a, b). The primer pair 2, which targeted the sequence starting from the insertion, can only clone the sequence from mutants. This indicates mutation at the transcriptional level, resulting in a single, premature, nonfunctional *pdzk1* mRNA expressed in the mutant (Fig. 7c). Importantly, there were no splice variants present (Fig. 7b). Comparing *pdzk1*-KO mutants with and without the nonsense-mediated decay interference (i.e., NMDi14 treatment), spatial frequency tuning functions (Figs. 8a–c), ERG (Figs. 8d–g), and densities of the four PDZK1-interacting molecules of interest (Figs. 8h–q) were not different between groups (Supplementary Table S7). These results suggest that there are no genetic mechanisms or splice variants compensating for the loss of *pdzk1* in these mutants.

Discussion

The human *PDZK1* gene is located on chromosome 1q21.1, a high-risk region for schizophrenia[31] and ASD.[32] It has been linked to altered contrast sensitivity, a visual endophenotype of both neurodevelopmental disorders, with each additional copy of the minor allele of the rs1797052 polymorphism in the regulatory region of *PDZK1* increasing sensitivity by more than half a standard deviation.[3] Our finding of enhanced contrast sensitivity in *pdzk1*-KO larvae (Figs. 2, 3) is consistent with these observations and highlights the cross-species conservation of this gene in visual function.

Our measurement of contrast response functions suggests that the improved spatial frequency tuning function in *pdzk1*-KO mutants is likely due to abnormal gain control (Fig. 3). Contrast gain control horizontally shifts the entire function without changing the function shape, indicating changes of contrast threshold for eliciting any response (i.e., contrast sensitivity). Response gain control is characterized by changes in the slope or maximum response without changing the baseline of the function.[33,34] We found no evidence of response gain changes in the contrast response functions of knockout fish (Fig. 3d; Supplementary Table S4). Instead, mutants showed significantly lower contrast thresholds (at 25°/s and 50°/s) compared to wild-type fish (Fig. 3e; Supplementary Table S4), indicating abnormal contrast gain rather than response gain in mutants. We note that these analyses were based on fitted functions, of which visual inspection does not clearly distinguish an improvement in threshold rather than gain. Increasing the resolution of contrasts tested, particularly around threshold contrast, would likely provide a more compelling distinction between reduced threshold versus increased gain in this analysis. An increased behavioral response may in some instances be the result of hyperactivity, but our locomotion test demonstrated that this is not the case in *pdzk1*-KO larvae: Both in the E3 medium used for embryonic husbandry and when exposed to a chemical stimulus (1.5% ethanol) that elicits increased motor activity in larval zebrafish, mutants showed consistently *reduced* locomotion relative to wild-type animals (Supplementary Fig. S3, Supplementary Table S1). One may be concerned that lower levels of spontaneous locomotion may paradoxically increase OMR by reducing variability among the *pdzk1*-KO group. However, although

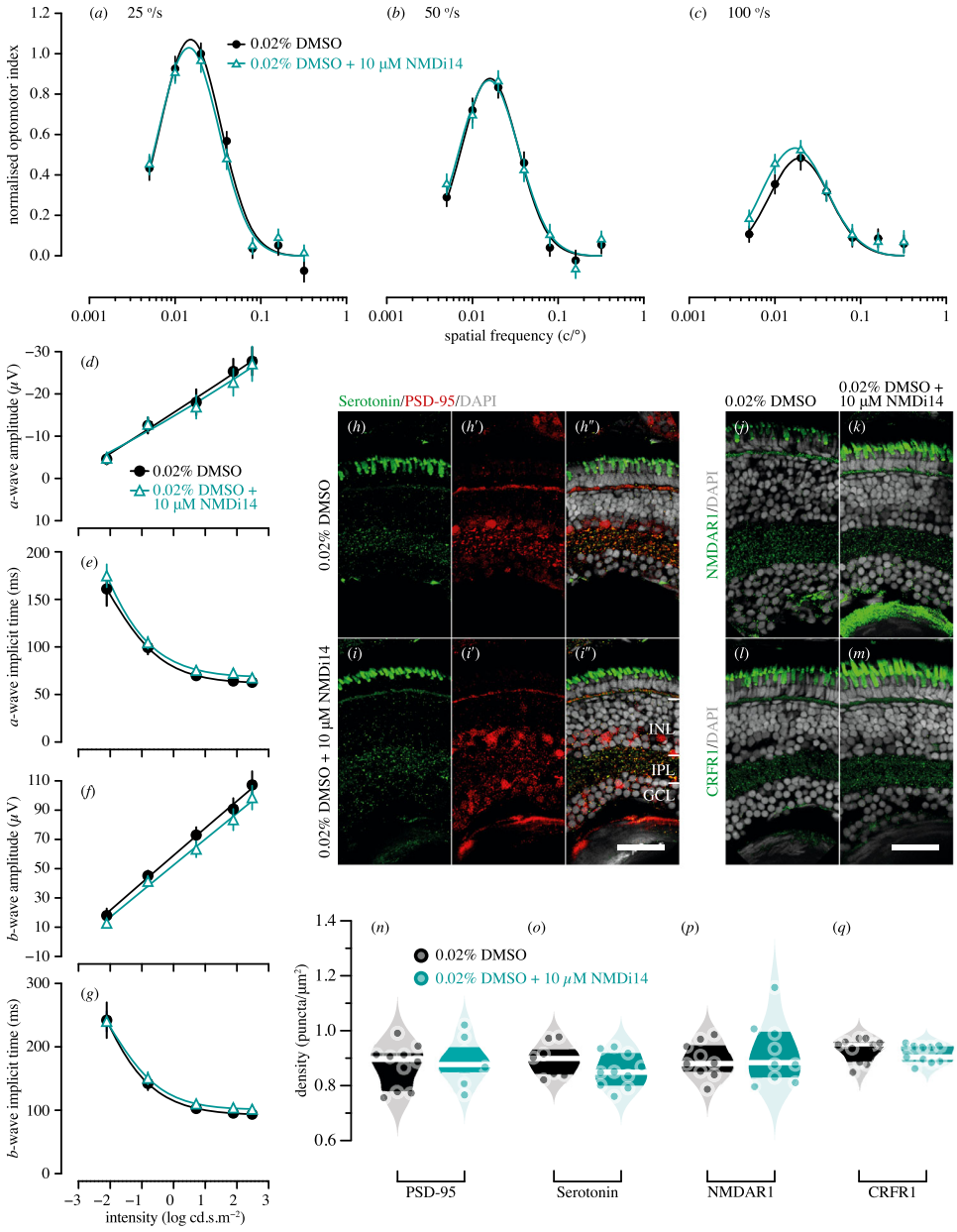

Figure 8. Genetic compensation tests for *pdzk1*-KO mutants at 7 dpf. Spatial frequency tuning functions were fitted by a log-Gaussian model for control (*pdzk1*-KO mutants treated with 0.02% DMSO; *black circles* and *lines*) and experimental groups (*pdzk1*-KO mutants treated with 0.02% DMSO and 10-µM NMDi14; *blue triangles* and *lines*) at (**a**) 25°/s, (**b**) 50°/s, and (**c**) 100°/s. ERG results were shown as the group average (±SEM) of (**d**) *a*-wave amplitude, (**e**) *a*-wave implicit time, (**f**) *b*-wave amplitude, and (**g**) *b*-wave implicit time for *pdzk1*-KO mutants treated with 0.02% DMSO (*filled black circles*) and mutants treated with 0.02% DMSO and 10-µM NMDi14 (*open cyan triangles*). Data were compared using two-way ANOVA; there were no significant differences. Lines were fit by a four-parameter sigmoidal function. For histological assessment, (**h–i″**) serotonin and PSD-95 were co-labeled in *green* and *red*, respectively, for both groups; (**j**, **k**) NMDAR1and (**l**, **m**) CRFR1 were labeled in *green*. For all images, nuclei were stained with DAPI, shown in *gray*. *Scale bars*: 25 µm. Violin plots show densities in the IPL of (**n**) PSD-95, (**o**) serotonin, (**p**) NMDAR1, and (**q**) CRFR1 for mutants treated with 0.02% DMSO (*black circles*) and mutants treated with 0.02% DMSO and 10-µM NMDi14 (*cyan circles*). Points represent data from individual retinas. *White lines* represent medians, and *dark bands* indicate interquartile ranges. Unpaired *t*-tests were performed with 10 or 11 retinas per group (see Supplementary Table S6).

adding a larger random component to the stimulus-evoked motion of each animal may increase the spatial dispersion of the wild-type group, it would not systematically bias the group centroid—this is our measure of OMR on each trial. It is also unlikely that the reduced OMR in wild-type larvae is attributable to an energy deficit from higher levels of spontaneous swimming. Contrast response functions did not saturate for either group even at full contrast (Figs. 3a–c), suggesting that the animals were not approaching any limit on energy expenditure.

The present results are consistent with the association between the human 1q21.1 genomic region containing *PDZK1* and risk of autism and schizophrenia. Infants at high risk for autism and people at high risk for psychosis also

show higher luminance contrast sensitivity,[35,36] although results differ between studies and may vary with age and experimental methods.[37,38] Altered contrast gain may originate in the retina via reduced inhibitory signals from amacrine cells onto parasol ganglion cells,[39] or it may occur in higher visual regions; however, the absence of a visual cortex in zebrafish, along with the electrophysiological findings of the present study, suggests that the effects of *PDZK1* variation are more likely retinal in origin. Our quantification showed an overall unchanged amacrine cell number in mutant retinas (Fig. 5g); future research may focus on inhibitory pathways in mutants at the subcellular or synaptic levels.

Our ERG results further corroborate that the neurodevelopmental risk gene *PDZK1* contributes to retinal function. With enhanced spatial contrast sensitivity in *pdzk1-KO* larvae compared to wild-types, one might expect larger ERG responses for mutants, but we found a reduction in the *b*-wave. This reduction agrees with the reduced scotopic ERG *b*-wave reported in individuals with schizophrenia and ASD.[40,41] Individuals with schizophrenia exhibit significantly decreased *a*-wave amplitudes[40]; however, the *b*-wave reduction in *pdzk1*-KO zebrafish was not due to photoreceptor deficits, as *a*-wave amplitudes did not differ between *pdzk1*-KO and wild-type larvae across all flash intensities (Fig. 4b; Supplementary Table S5). In contrast, the ERG phenotype observed in *pdzk1*-KO mutants may be more similar to those with ASD, who show no significant changes in *a*-wave amplitude,[41] although further research into the developmental trajectory of the ERG changes is needed. Although *pdzk1*-KO mutants presented altered retinal function and contrast sensitivity similar to that exhibited by some individuals with neurodevelopmental disorders, the role of *PDZK1* in the visual phenotypes of ASD and schizophrenia is currently unknown.

Selective attenuation of the *b*-wave at higher stimulus intensities (1.89 and 2.48 log cd·s·m^{-2}) in *pdzk1*-KO fish suggests that *pdzk1* disruption affects either bipolar cells directly or via third-order neurons (i.e., amacrine and ganglion cells). If enhanced behavioral contrast sensitivity in *pdzk1*-KO zebrafish arises from deficits of inhibitory mechanisms, altered bipolar cell responses underlying the *b*-wave may be modulated by a more generalized change in retinal inhibition. In rodents, antagonist blockage or genetic knockout of the gamma aminobutyric acid ($GABA_c$) receptor, a key inhibitory receptor on bipolar cells, leads to a reduced ERG *b*-wave but increased spontaneous and light-evoked activity in retinal ganglion cells.[42–44] How PDZK1 might be involved in the crosstalk among bipolar, amacrine, and ganglion cells remains to be investigated.

Although the observed *b*-wave deficit points to bipolar or third-order retinal dysfunction, there could be other potential causes. PDZK1 may contribute to microvillus formation in the retinal pigment epithelium (RPE) through its interaction with ezrin/radixin/moesin (ERM), binding phosphoprotein 50 kDa (EBP50) and ezrin.[45,46] RPE apical microvilli interdigitate with outer segments of adjacent photoreceptors, involved in essential functions of the RPE for retinal homeostasis (e.g., phagocytosis of photoreceptor debris, nutrient transportation into retina, removal of photoreceptor waste products, visual pigment regeneration).[45,47] Therefore, loss of PDZK1 may disrupt retinal homeostasis and thus retinal function; however, in this case, one might also expect altered *a*-wave responses, which were not observed. Knockout of murine Pdzk1 leads to reduced posttranscriptional expression of scavenger receptor class B type I (SR-BI), altering lipid metabolism for high-density lipoprotein (HDL) in total plasma.[48] Plasma HDL has been associated with age-related macular degeneration,[49,50] linking PDZK1 via SR-BI to a pathogenic mechanism of eye disease. PDZK1 may also maintain neural homeostasis by increasing the activity of glutamate transporter excitatory amino acid carrier 1 (EAAC1) on the cell membrane.[51] Cross-talk among EAAC1, NMDARs, and α-amino-3-hydroxy-5-methyl-4-isoxazolepropionic acid (AMPA) receptors tightly modulates the extracellular concentration of glutamate to avoid excitotoxicity.[52] In mice, EAAC1 deficiency results in excitotoxic retinal damage, specifically ganglion cell loss.[53] Loss of PDZK1 may lead to dysfunction of the inner retina by this indirect route.

Our histological analyses indicated that there was a minor reduction in retinal length in mutant retinas, with no other morphological changes observed (Figs. 5c–g; Supplementary Table S6). Despite this, there was no reduction in overall retinal size; this may be because mutants with reduced retinal length had correspondingly thicker retinas (Supplementary Fig. S5). Although we carefully ensured that images were taken within two sections of the optic nerve, it is possible that the sectioning angle could affect this result. Overall, our data indicated that compared to wild-types, *pdzk1*-KO larvae might have slightly shorter retinas, but retinal cellular organization and morphology are generally intact. Further investigation is required to confirm any link between this morphological change and the altered behavioral and functional phenotypes of mutants.

The density in the IPL of four molecules of particular interest was unchanged in the mutant retinas (Figs. 6f, g; Supplementary Table S2). We were not able to examine an effect of *pdzk1* knockout on receptors in the OPL, as the zebrafish OPL is too thin for effective quantification with the available imaging approaches. Previous studies have shown that early in disease progression (e.g., in diabetes) or under physical stress (e.g., high intraocular pressure), ERG abnormalities can manifest without apparent structural changes.[54,55] However, our analysis of synaptic molecular density from 7 dpf to 8 wpf suggested that progressive changes in the tested molecules are unlikely to underlie altered function in *pdzk1*-KO mutants.

We have confirmed the absence of a genetic mechanism for histological phenotype rescue for *pdzk1*-KO mutants. Our data showed that variant splices of *pdzk1* mRNA are absent in mutant fish, with a single *pdzk1* mRNA being expressed with the stop codon cassette, leading to a premature, nonfunctional Pdzk1 (Figs. 7b, c). Multilevel analysis (OMR, ERG, and histology) of *pdzk1*-KO mutants treated with NMD interference (NMDi14) demonstrated that compensatory genetic pathways are not present in our *pdzk1*-KO fish (Fig. 8; Supplementary Table S6). We are therefore confident our histological results are robust.

Ultimately, our histological data provide evidence that, although PDZK1 may associate with synaptic proteins, it is not necessary for their clustering into synaptic puncta. We note that the PDKZ1-associated molecules considered to be of interest in this study were identified by co-localization or in vitro cell culture[5,12]; however, the role of PDZK1 and the proteins it interacts with in vivo may be different. Further histological research could focus on other PDZK1-interacting molecules such as SynGAP1 and KLHL17. Higher power imaging of individual subtypes of neurons may reveal very specific contributions of PDZK1 to the maintenance of

Investigative Ophthalmology & Visual Science

cellular morphology and synaptic distribution within select visual pathways. The impact of *pdzk1* knockout on the RPE and ganglion cells is also a potential avenue for future investigation.

Conclusions

Our study supports an association between PDZK1 and visual function. The present behavioral results are consistent with altered contrast gain control. Electrophysiology reveals a reduced ERG *b*-wave amplitude, indicating deficits in the inner retina in *pdzk1*-KO zebrafish. This study highlights the utility of the zebrafish model in assessing the role of genes associated with abnormal visual function.

Acknowledgments

The authors thank the staff of the zebrafish facility at the Walter and Eliza Hall Institute of Medical Research for animal maintenance, the Biological Optical Microscopy Platform of the Melbourne Advanced Microscopy Facility for providing instruments for confocal imaging, and Steven D. Leach, MD, of Johns Hopkins University for providing the Tg(*ptf1a*:*GFP*) zebrafish line.

Supported by a grant from the Melbourne Neuroscience Institute (to PTG, PRJ, BVB). PTG was supported by a Discovery Early Career Researcher Award from the Australian Research Council (DE160100125).

Disclosure: **J. Xie,** None; **P.R. Jusuf,** None; **B.V. Bui,** None; **S. Dudczig,** None; **T.E. Sztal,** None; **P.T. Goodbourn,** None

References

1. Kéïta L, Guy J, Berthiaume C, Mottron L, Bertone A. An early origin for detailed perception in Autism Spectrum Disorder: Biased sensitivity for high-spatial frequency information. *Sci Rep*. 2014;4:5475.
2. Kéri S, Antal A, Szekeres G, Benedek G, Janka Z. Spatiotemporal visual processing in schizophrenia. *J Neuropsychiatry Clin Neurosci*. 2002;14(2):190–196.
3. Goodbourn PT, Bosten JM, Bargary G, Hogg RE, Lawrance-Owen AJ, Mollon JD. Variants in the 1q21 risk region are associated with a visual endophenotype of autism and schizophrenia. *Genes Brain Behav*. 2014;13(2):144–151.
4. Ardura JA, Friedman PA. Regulation of G protein-coupled receptor function by Na+/H+ exchange regulatory factors. *Pharmacol Rev*. 2011;63(4):882–900.
5. Chen Y, Li M. Interactions between CAP70 and actinfilin are important for integrity of actin cytoskeleton structures in neurons. *Neuropharmacology*. 2005;49(7):1026–1041.
6. Gomperts SN. Clustering membrane proteins: It's all coming together with the PSD-95/SAP90 protein family. *Cell*. 1996;84(5):659–662.
7. Chen Y, Derin R, Petralia RS, Li M. Actinfilin, a brain-specific actin-binding protein in postsynaptic density. *J Biol Chem*. 2002;277(34):30495–30501.
8. Feyder M, Karlsson R-M, Mathur P, et al. Association of mouse Dlg4 (PSD-95) gene deletion and human DLG4 gene variation with phenotypes relevant to autism spectrum disorders and Williams' syndrome. *Am J Psychiatry*. 2010;167(12):1508–1517.
9. Südhof TC. Neuroligins and neurexins link synaptic function to cognitive disease. *Nature*. 2008;455(7215):903–911.
10. Daw NW, Stein PSG, Fox K. The role of NMDA receptors in information processing. *Annu Rev Neurosci*. 1993;16:207–222.
11. Butler PD, Silverstein SM, Dakin SC. Visual perception and its impairment in schizophrenia. *Biol Psychiatry*. 2008;64(1):40–47.
12. Walther C, Caetano FA, Dunn HA, Ferguson SSG. PDZK1/NHERF3 differentially regulates corticotropin-releasing factor receptor 1 and serotonin 2a receptor signaling and endocytosis. *Cell Signal*. 2015;27(3):519–531.
13. Ramot A, Jiang Z, Tian J-B, et al. Hypothalamic CRFR1 is essential for HPA axis regulation following chronic stress. *Nat Neurosci*. 2017;20(3):385–388.
14. Magalhaes AC, Holmes KD, Dale LB, et al. CRF receptor 1 regulates anxiety behavior via sensitization of 5-HT2 receptor signaling. *Nat Neurosci*. 2010;13(5):622–629.
15. London A, Benhar I, Schwartz M. The retina as a window to the brain: from eye research to CNS disorders. *Nat Rev Neurol*. 2013;9(1):44–53.
16. Ketharnathan S, Leask M, Boocock J, et al. A non-coding genetic variant maximally associated with serum urate levels is functionally linked to HNF4A-dependent PDZK1 expression. *Hum Mol Genet*. 2018;27(22):3964–3973.
17. Gagnon JA, Valen E, Thyme SB, et al. Efficient mutagenesis by Cas9 protein-mediated oligonucleotide insertion and large-scale assessment of single-guide RNAs. *PLoS One*. 2014;9(5):e98186.
18. Jusuf PR, Almeida AD, Randlett O, Joubin K, Poggi L, Harris WA. Origin and determination of inhibitory cell lineages in the vertebrate retina. *J Neurosci*. 2011;31(7):2549–2562.
19. Jusuf PR, Harris WA. Ptf1a is expressed transiently in all types of amacrine cells in the embryonic zebrafish retina. *Neural Dev*. 2009;4:34.
20. Xie J, Goodbourn PT, Bui BV, Sztal TE, Jusuf PR. Correspondence between behavioral, physiological, and anatomical measurements of visual function in inhibitory neuron-ablated zebrafish. *Invest Ophthalmol Vis Sci*. 2019;60(14):4681–4690.
21. Xie J, Jusuf PR, Bui BV, Goodbourn PT. Experience-dependent development of visual sensitivity in larval zebrafish. *Sci Rep*. 2019;9(1):1893.
22. Lu Z-L, Dosher B. *Visual Psychophysics: From Laboratory to Theory*. Cambridge, MA: MIT Press; 2013.
23. Sztal TE, Ruparelia AA, Williams C, Bryson-Richardson RJ. Using touch-evoked response and locomotion assays to assess muscle performance and function in zebrafish. *J Vis Exp*. 2016;116:54431.
24. Xie J, Jusuf PR, Goodbourn PT, Bui BV. Electroretinogram recording in larval zebrafish using a novel cone-shaped sponge-tip electrode. *J Vis Exp*. 2019;145:e59487.
25. Schindelin J, Arganda-Carreras I, Frise E, et al. Fiji: an open-source platform for biological-image analysis. *Nat Methods*. 2012;9(7):676–682.
26. Quintana DS, Williams DR. Bayesian alternatives for common null-hypothesis significance tests in psychiatry: a non-technical guide using JASP. *BMC Psychiatry*. 2018;18(1):178.
27. El-Brolosy MA, Kontarakis Z, Rossi A, et al. Genetic compensation triggered by mutant mRNA degradation. *Nature*. 2019;568(7751):193–197.
28. Lockwood B, Bjerke S, Kobayashi K, Guo S. Acute effects of alcohol on larval zebrafish: a genetic system for large-scale screening. *Pharmacol Biochem Behav*. 2004;77(3):647–654.
29. Mou H, Smith JL, Peng L, et al. CRISPR/Cas9-mediated genome editing induces exon skipping by alternative splicing or exon deletion. *Genome Biol*. 2017;18(1):108.

30. Sharpe JJ, Cooper TA. Unexpected consequences: exon skipping caused by CRISPR-generated mutations. *Genome Biol*. 2017;18(1):109.
31. Zheng Y, Wang X, Gu N, et al. A two-stage linkage analysis of Chinese schizophrenia pedigrees in 10 target chromosomes. *Biochem Biophys Res Commun*. 2006;342(4):1049–1057.
32. Casey JP, Magalhaes T, Conroy JM, et al. A novel approach of homozygous haplotype sharing identifies candidate genes in autism spectrum disorder. *Hum Genet*. 2012;131(4):565–579.
33. Soma S, Shimegi S, Suematsu N, Sato H. Cholinergic modulation of response gain in the rat primary visual cortex. *Sci Rep*. 2013;3:1138.
34. Soma S, Shimegi S, Suematsu N, Tamura H, Sato H. Modulation-specific and laminar-dependent effects of acetylcholine on visual responses in the rat primary visual cortex. *PLoS One*. 2013;8(7):e6843.
35. Kéri S, Benedek G. Visual contrast sensitivity alterations in inferred magnocellular pathways and anomalous perceptual experiences in people at high-risk for psychosis. *Vis Neurosci*. 2007;24(2):183–189.
36. McCleery JP, Allman E, Carver LJ, Dobkins KR. Abnormal magnocellular pathway visual processing in infants at risk for autism. *Biol Psychiatry*. 2007;62(9):1007–1014.
37. Guy J, Mottron L, Berthiaume C, Bertone A. The developmental trajectory of contrast sensitivity in autism spectrum disorder. *Autism Res*. 2016;9(8):866–878.
38. Koh HC, Milne E, Dobkins K. Spatial contrast sensitivity in adolescents with autism spectrum disorders. *J Autism Dev Disord*. 2010;40(8):978–987.
39. Marshak DW, Yamada ES, Bordt AS, Perryman WC. Synaptic input to an ON parasol ganglion cell in the macaque retina: a serial section analysis. *Vis Neurosci*. 2002;19(3):299–305.
40. Demmin DL, Davis Q, Roché M, Silverstein SM. Electroretinographic anomalies in schizophrenia. *J Abnorm Psychol*. 2018;127(4):417–428.
41. Creel DJ, Crandall AS, Pingree C, Ritvo ER. Abnormal electroretinograms in autism. *Clin Vis Sci*. 1989;4:85–88.
42. Kapousta-Bruneau NV. Opposite effects of GABA(A) and GABA(C) receptor antagonists on the b-wave of ERG recorded from the isolated rat retina. *Vision Res*. 2000;40(13):1653–1665.
43. Lukasiewicz PD, Eggers ED, Sagdullaev BT, McCall MA. GABAC receptor-mediated inhibition in the retina. *Vision Res*. 2004;44(28):3289–3296.
44. Wang J, Mojumder DK, Yan J, et al. In vivo electroretinographic studies of the role of GABAC receptors in retinal signal processing. *Exp Eye Res*. 2015;139:48–63.
45. Bonilha VL, Rayborn ME, Bhattacharya SK, et al. The retinal pigment epithelium apical microvilli and retinal function. In: Hollyfield JG, Anderson RE, LaVail MM , eds. *Retinal Degenerative Diseases*. Boston, MA: Springer; 2006:519–524.
46. LaLonde DP, Garbett D, Bretscher A, Yap A. A regulated complex of the scaffolding proteins PDZK1 and EBP50 with ezrin contribute to microvillar organization. *Mol Biol Cell*. 2010;21(9):1519–1529.
47. Bok D. The retinal pigment epithelium: a versatile partner in vision. *J Cell Sci*. 1993;17:189–195.
48. Kocher O, Yesilaltay A, Cirovic C, Pal R, Rigotti A, Krieger M. Targeted disruption of the PDZK1 gene in mice causes tissue-specific depletion of the high density lipoprotein receptor scavenger receptor class B type I and altered lipoprotein metabolism. *J Biol Chem*. 2003;278(52):52820–52825.
49. Cougnard-Grégoire A, Delyfer M-N, Korobelnik J-F, et al. Elevated high-density lipoprotein cholesterol and age-related macular degeneration: the Alienor study. *PLoS One*. 2014;9(3):e90973.
50. Ishida BY, Duncan KG, Bailey KR, Kane JP, Schwartz DM. High density lipoprotein mediated lipid efflux from retinal pigment epithelial cells in culture. *Br J Ophthalmol*. 2006;90(5):616–620.
51. D' Amico A, Soragna A, Di Cairano E, et al. The surface density of the glutamate transporter EAAC1 is controlled by interactions with PDZK1 and AP2 adaptor complexes. *Traffic*. 2010;11(11):1455–1470.
52. Cabrera-Pastor A, Taoro L, Llansola M, Felipo V. Roles of the NMDA receptor and EAAC1 transporter in the modulation of extracellular glutamate by low and high affinity AMPA receptors in the cerebellum in vivo: differential alteration in chronic hyperammonemia. *ACS Chem Neurosci*. 2015;6(12):1913–1921.
53. Harada T, Harada C, Nakamura K, et al. The potential role of glutamate transporters in the pathogenesis of normal tension glaucoma. *J Clin Invest*. 2007;117(7):1763–1770.
54. Tzekov R, Arden GB. The electroretinogram in diabetic retinopathy. *Surv Ophthalmol*. 1999;44(1):53–60.
55. Bach M. Electrophysiological approaches for early detection of glaucoma. *Eur J Ophthalmol*. 2001;11(suppl 2):S41–S49.

Investigative Ophthalmology & Visual Science